Hindawi
Journal of Sensors
Volume 2024, Article ID 6834284, 17 pages
https://doi.org/10.1155/2024/6834284

*Research Article*

# A High Degree of Freedom Radiation Near-Field Source Localization Algorithm with Gain–Phase Error

**Qi Zhang**,[1] **Wenxing Li**,[1] **Si Li**,[2] **and Yunlong Mao**[2]

[1]*The College of Information and Communication Engineering, Harbin Engineering University, Harbin 150001, China*
[2]*The School of Electronics and Information, Jiangsu University of Science and Technology, Zhenjiang, Jiangsu 212100, China*

Correspondence should be addressed to Si Li; lisi0511@just.edu.cn

Received 10 August 2023; Revised 19 December 2023; Accepted 23 December 2023; Published 23 January 2024

Academic Editor: Kathiravan Srinivasan



The limitation of the number of estimable sources in the localization of radiation near-field sources with gain–phase error is examined in this paper. When only the reference element has no gain–phase error, a new method based on an accurate model is proposed to enhance the maximum number of estimable sources. Based on the location parameter details of the auxiliary source, the method first derives the gain–phase error estimate matrix. Second, the source steering vector including errors is estimated using the total least square estimating signal parameter via rotational invariance techniques (TLS-ESPRIT), and the time-shifted data matrix is built utilizing the space–time combination idea, thus increasing the degree of freedom of the array. Then, the source steering vector containing the error is modified by the error compensation matrix constructed according to the moment of gain–phase error estimation. Finally, the estimated values of the source position parameters are obtained by using the closed formula of the gain phase of the modified source steering vector and the source position parameters. The experimental results show that the maximum estimable source number of the proposed algorithm is significantly improved compared with the previous results when only the reference array element has no gain–phase error. When the array number is 5 and 9, the maximum estimable source number of the algorithm is 9 and 17, respectively.

## 1. Introduction

Source localization is a research branch of array signal processing, and it plays an important role in radar, electronic monitoring, navigation, aerospace, and medical imaging [1–3]. In the initial stage of source location research, the direction of incoming wave is mainly estimated for radiation far-field (RFF) sources and a large number of related algorithms are proposed [4–8]. With the rapid development of 5G and MIMO technologies [8, 9], the space electromagnetic field environment becomes more complex, and the distances between some sources and arrays are less than the Rayleigh distance. The location of such sources also needs to consider the estimation of source range parameters. In recent years, the location parameter estimation of radiation near-field (RNF) sources or radiation mixed sources has become a key research direction. Among the existing results, most of them are based on the ideal environment of the RNF source or the mixed source localization algorithm in the radiation field [10–15].

In practical engineering applications, due to various errors are inevitable, the actual array flow pattern often has a certain degree of deviation or disturbance, so the performance of the RNF source localization algorithm based on the ideal environment seriously deteriorates or even fails. In view of the existence of sensor position error [16], mutual coupling between array elements [17, 18] or amplitude phase error [19], it is of great significance to study the RNF source localization algorithm. At present, some related algorithms have been proposed [19–24]. The methods of these algorithms to solve the amplitude phase error can be divided into two categories:

(1) The auxiliary array element method [20–24]: first, it is assumed that some elements have been calibrated. Then a special fourth-order cumulant matrix about the calibrated array is constructed or the relevant second order moments are constructed based on calibrated arrays. Finally, the source location parameters

are estimated by the rotationally invariant subspace method. This method has at least three correction elements and has high computational complexity.

(2) The priority estimation RFF source method [19]: first, the incoming direction of the RFF source is estimated according to the spatial spectrum estimation method. Then the error parameters are calculated according to the angle estimates of the radiating far-field source. Finally, a special matrix related to RNF is constructed and the RNF source location parameters are estimated.

In recent years, some results have been proposed for mix RNF and RFF localization with amplitude and phase errors. The characteristics of the far-field source steering vector and the MUSIC algorithm are used to estimate the amplitude phase error of the array in [19], and then the MUSIC algorithm is used again to estimate the position parameters of the RNF source. Although, the method does not use calibration array to avoid the influence of amplitude phase error, but is limited by the assistance of far-field sources. A special method based on electromagnetic vector sensor combined with polarization to solve the effect of amplitude phase error in [20], but the source position parameter estimation without spectrum search is closely related to the particularity of the array element. In [21, 23, 24], the core of source location parameter estimation methods is the combination of special high-order cumulants and ESPRIT or MUSIC, which mainly constructs the required special high-order moments according to the adopted methods. In order to avoid the construction of special high-order moments, the DOA estimation using sparse total least squares algorithm is proposed in [22], and the source position parameter estimation is first realized and then the amplitude phase error is estimated. In the above algorithms, the core methods used to estimate the information source location parameters still adopt the idea of ESPRIT and MUSIC. The maximum estimable source number of the above algorithm is limited by the data covariance matrix, resulting in the maximum estimable source must be less than the total number of elements. However, the number of sources to be estimated in a real-world environment is a factor of uncertainty. When the total number of sources is greater than the number of array elements, the existing RNF source location algorithm cannot achieve the estimation of all source location parameters under nonideal conditions. Therefore, the research about increasing the maximum number of estimable sources in the algorithm is significant.

On the other hand, the amplitude of the RNF source steering vector in the precise model has a path loss and the phase is nonlinear. Most of the above RNF source localization algorithms use the Fresnel approximation model to estimate the location parameters of the RNF source [19–22]. The amplitude of the source steering vector based on the Fresnel model is assumed to be 1, and the phase is in the form of a quadratic sum. However, there is a model mismatch between the Fresnel model and the precise signal model, and nonrandom errors are introduced into the array flow pattern. Therefore, the RNF source localization algorithm based on Fresnel model cannot accurately estimate the source location parameter estimation in the actual environment.

The existing RNF source location parameter estimation algorithms have certain restrictions when there is amplitude-phase error, that is, the maximum estimated number of sources is limited by the total number of elements. To address this limitation, we propose an RNF source location algorithm based on auxiliary source and delay. Consider an RNF source with known positional parameters. The amplitude-phase error of each element can be estimated by using this auxiliary source and a calibration matrix of amplitude phase error is constructed. In addition, we use the delay method to increase the maximum estimable source number of the algorithm and avoid the construction of special high-priced cumulants. We use the data received by the array and the data after the delay to constructed the matrix beam and obtain the source location parameters are estimated by total least square estimating signal parameter via rotational invariance techniques (TLS-ESPRIT) algorithm.

Compared with the existing methods, the main contributions of this paper are as follows:

(i) It increases the maximum number of estimable sources without increasing the number of elements or increasing the spacing between adjacent element.

(ii) It adopts the space–time combination method and the subspace fitting method to construct the received data matrix with the same structure, which avoids the generation of special fourth-order cumulants.

(iii) The exact model of nonuniform linear array is used to avoid the mismatch problem of Fresnel model. In addition, the spacing between adjacent arrays is not limited to less than a quarter of the wavelength or the array is symmetrical.

The remaining article is structured as follows: Section 2 introduces the accurate model of RNF source when there are amplitude and phase errors. Section 3 introduces the source location parameter estimation method combined with auxiliary source and delay method. In Section 4, the localization performance of the proposed algorithm is analyzed from three aspects: computational complexity, maximum estimable source number, and hybrid source localization capability. The simulation results of the proposed algorithm and other algorithms are given in Section 5. Finally, Section 6 offers the summary of this paper and the prospect of future related work according to the simulation results.

Throughout the paper, the $(\,)^T, \cdot, (\,)^H$, and $(\,)^{-1}$ denote transpose, point multiplication, conjugate transpose, and inverse, respectively. $\angle$A represents the angle corresponding to phase A; $[\mathbf{A} \mid \mathbf{B}]$ denotes the combination of $\mathrm{K} \times \mathrm{K}$ matrix $\mathbf{A}$ and $\mathrm{K} \times \mathrm{K}$ matrix $\mathbf{B}$ into a new $2\mathrm{K} \times \mathrm{K}$ matrix; $||$ the absolute value; diag( ) the diagonal matrix; span{ } the expansion space; arcsin( ) is inverse-sine function and argmin( ) the minimum phase of a complex number. $\boldsymbol{I}_K$ denotes the $\mathrm{K} \times \mathrm{K}$ identity matrix. $\boldsymbol{E}$ is taking the mean of the data.

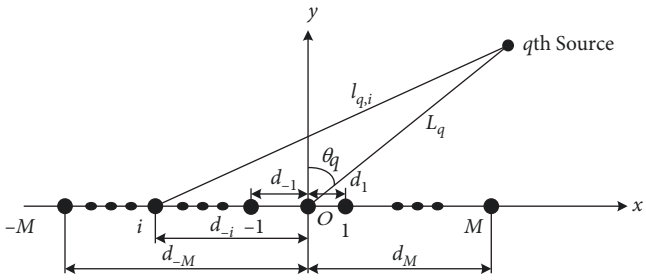


FIGURE 1: Nonuniform linear array model without magnitude phase error.

## 2. Array Model with Gain–Phase Error

Assume $Q$ randomly distributed narrowband and independent RNF signals impinge on a nonuniform linear array composed of $N$ $(N = 2M + 1, M \in \mathbf{Z}+)$ elements, where $M$ is the number of array elements on one side of the coordinate origin and the elements arranged on the $X$-axis, as illustrated in Figure 1. The $M + 1$th element, which is called the reference element, is located at the origin of the Cartesian coordinate and serves as a reference for magnitude and phase. Narrowband RNF sources are nonzero peak stationary random processes, with $(\theta_p,\ L_p)$ denoting the $q$-th source position. $\theta_q \in (-\pi/2,\ \pi/2)$ is the angle formed by the incoming direction of the source and the normal location of the reference element, and it is referred to as the direction of arrival. The source array distance is $L_q \in [0.62\sqrt{D^3/\lambda},\ 2D^2/\lambda]$, which is the distance from the source to the reference element, where $\lambda$ is the wavelength and $D$ is the array aperture. The distance from various sources to various elements varies, with the distance from the $q$-th source to the $i$-th element given as follows:

$$l_{i,q} = \sqrt{(L_q \sin\theta_q)^2 + (L_q \cos\theta_q - d_i)^2}, \tag{1}$$

where $d_i$ is the position coordinate of $i$-th element.

In ideal case, the magnitude–phase factor between the $i$-th element and the $q$-th source can be summarized by the following equation:

$$a_i(\theta_q,\ L_q) = \eta_{i.q} e^{-j\varphi_{i,q}} = \frac{L_q}{l_{i,q}} e^{-j\frac{2\pi}{\lambda}(L_q - l_{i,q})}, \tag{2}$$

where $\eta_{i.q} = L_q/l_{i,q}$ is referred to as the spatial magnitude factor and $\varphi_{i,q} = 2\pi(L_q - L_{i,q})/\lambda$ is the spatial phase factor. The data that the $i$-th element receives from the $q$-th source at time $t$ can represent as follows:

$$x_i(t) = \sum_{q=1}^{Q} a_i(\theta_q,\ L_q) s_q(t) + n_i(t), \tag{3}$$

where $s_q(t)$ represents the spatial signal of $q$th source, and the noise of $i$th element is represented by $n_i(t)$ at time $t$. The representation of the data it has received is as follows:

$$\boldsymbol{X}(t) = \sum_{q=1}^{Q} \boldsymbol{a}(\theta_q,\ l_q) s_q(t) + \boldsymbol{n}(t) = \boldsymbol{A}\boldsymbol{S}(t) + \boldsymbol{N}(t), \tag{4}$$

where $\boldsymbol{S}(t) = [s_1(t),\ \ldots,\ s_Q(t)]^T$ is the $Q \times 1$ signal vector and $\boldsymbol{N}(t) = [n_{-M}(t),\ \ldots,\ n_0(t),\ \ldots,\ n_M(t)]^T$ denotes the $N \times 1$ additive and uncorrelated noise vector. $\boldsymbol{A} = [\boldsymbol{a}(\theta_1,\ l_1),\ \ldots,\ \boldsymbol{a}(\theta_Q,\ l_Q)]$ is a $N \times Q$ array flow pattern matrix, in which the data steering vector of the $q$th source is described as follows:

$$\begin{aligned}\boldsymbol{a}(\theta_q, L_q) &= [a_{-M}(\theta_q,\ L_q),\ \ldots,\ a_0(\theta_q,\ L_q),\ \ldots,\ a_M(\theta_q,\ L_q)]^T \\ &= [\eta_{-M,q} e^{j\varphi_{-M,q}},\ \ldots,\ \eta_{0,q} e^{j\varphi_{0,q}},\ \ldots,\ \eta_{M,q} e^{j\varphi_{M,q}}]^T.\end{aligned} \tag{5}$$

In practice, the gain–phase error is caused by the irregularity of the gain of amplifier in the array receiving channel. The steering vector of the array receiving the $q$-th source is now written as follows:

$$\begin{aligned}\widehat{\boldsymbol{a}}(\theta_q, L_q) &= [\Gamma_{-M} a_{-M}(\theta_q,\ L_q),\ \ldots,\ \Gamma_0 a_0(\theta_q,\ L_q),\ \ldots,\ \Gamma_M a_M(\theta_q,\ L_q)]^T \\ &= \Gamma \boldsymbol{a}(\theta_q,\ L_q),\end{aligned} \tag{6}$$

where $\Gamma = \mathrm{diag}(\Gamma_{-M},\ \ldots,\ \Gamma_0,\ \ldots,\ \Gamma_M)$ is a $N \times N$ gain–phase error matrix and $\Gamma_i$ is the gain–phase error factor of the $i$th element. The magnitude phase factor of the reference element is $a_0(\theta_q,\ L_q)$, and the gain–phase error factor $\Gamma_0$ of reference element is assumed to be 1. In the presence of gain–phase errors, the array manifold is represented as follows:

$$\begin{aligned}\widehat{\boldsymbol{A}} &= [\widehat{\boldsymbol{a}}(\theta_1,\ l_1),\ \widehat{\boldsymbol{a}}(\theta_2,\ l_2),\ \ldots,\ \widehat{\boldsymbol{a}}(\theta_Q,\ l_Q)] \\ &= \Gamma \boldsymbol{A}.\end{aligned} \tag{7}$$

The actual received data of array is represented as follows:

$$\begin{aligned}\widehat{\boldsymbol{X}}(t) &= \sum_{q=1}^{Q} \widehat{\boldsymbol{a}}(\theta_q,\ l_q) s_q(t) + \boldsymbol{n}(t) \\ &= \Gamma \boldsymbol{A}\boldsymbol{S}(t) + \boldsymbol{N}(t).\end{aligned} \tag{8}$$

*Note.* The total number of sources must be precisely estimated as a prior condition for subspace technology in the source localization issue. The approach in [25] is equally applicable to estimating the quantity of mixed and RNF sources, as evidenced by a large number of simulation results in [24]. The number of sources Q has been precisely determined in this study to help the next method. Furthermore, unlike [19–22, 26], this research uses a nonuniform linear array based on an accurate model to eliminate the model mismatch problem produced by the simplified model, and the array spacing is not restricted by the quarter wavelength.

## 3. Gain Phase Error Estimation and Source Location

The stages of the RNF source localization technique with a high array degree of freedom in the presence of gain–phase errors are provided in this section. The estimation of the gain–phase error matrix and enhancement of the array degrees of freedom are accomplished by the proposed method using the auxiliary source (AS) approach and the space–time combination method. The following three phases make up the bulk of the proposed algorithm:

(i) Estimate the gain–phase error factor on each element except the reference element according to the auxiliary source position information.

(ii) Time-shifting was used to create a new data set about the received data, and TLS-ESPRIT was used to calculate the array steering vector with gain–phase error.

(iii) Accurate source position estimate is achieved by combining the necessary formulas, and accurate steering vector estimation is achieved by estimating the gain–phase error factor and the steering vector containing error.

*3.1. Estimation of Gain Phase Error Matrix.* The auxiliary source method is used to estimate the gain–phase error on the array. Assume that there is an AS with known location information in RNF, and its location is $(\tilde{\theta}, \tilde{L})$. The data received by the array about the AS are expressed as follows:

$$\begin{aligned}\widetilde{\boldsymbol{X}}(t) &= \widehat{\boldsymbol{a}}\left(\widetilde{\theta}, \widetilde{l}\right)\widetilde{s}(t) + \boldsymbol{n}(t) \\ &= \Gamma\widetilde{\boldsymbol{A}}\widetilde{\boldsymbol{S}} + \boldsymbol{N},\end{aligned} \tag{9}$$

where $\tilde{s}(t)$ is the information of AS at the t time, $\boldsymbol{n}(t)$ is an $N\times 1$ noise vector, and $\widehat{\boldsymbol{a}}(\tilde{\theta}, \tilde{l})$ is an $N\times 1$ steering vector with a gain–phase error, and it can be expressed as the product of the error matrix and the ideal AS steering vector, which is expressed as follows:

$$\widehat{\boldsymbol{a}}\left(\widetilde{\theta}, \widetilde{l}\right) = \Gamma\boldsymbol{a}\left(\widetilde{\theta}, \widetilde{l}\right). \tag{10}$$

Since the position parameters of the AS are known, the steering vector of the ideal AS can be calculated by theoretical formula. Therefore, the error factor estimation can be realized only by the steering vector estimation of the AS containing errors. A subspace fitting method is used to estimate AS steering vector with errors. The covariance matrix of the received data about the AS is as follows:

$$\widetilde{\boldsymbol{R}} = \widetilde{\boldsymbol{X}}\widetilde{\boldsymbol{X}}/\mathrm{K} = \Gamma\widetilde{\boldsymbol{A}}\widetilde{\boldsymbol{R}}_S\widetilde{\boldsymbol{A}}^H\Gamma^H + \sigma_n^2\boldsymbol{I}_N, \tag{11}$$

where $K$ is the number of snapshot. The eigenvalue decomposition (EVD) of $\tilde{\boldsymbol{R}}$ can be obtained as follows:

$$\widetilde{\boldsymbol{R}} = \widetilde{\boldsymbol{U}}_S\widetilde{\Lambda}_S\widetilde{\boldsymbol{U}}_S^H + \boldsymbol{U}_N\Lambda_N\boldsymbol{U}_N^H, \tag{12}$$

where $\tilde{\Lambda}_S = \lambda_1$ is the maximum eigenvalue, and $\Lambda_N = \mathrm{diag}(\lambda_2, \ldots, \lambda_N)$ is a $N-1\times N-1$ diagonal matrix of $N-1$ smaller eigenvalues. $\tilde{\boldsymbol{U}}_S = [\boldsymbol{e}_1]$ is the $N\times 1$ signal subspace composed of eigenvectors corresponding to the largest eigenvalue, and $\boldsymbol{U}_N = [\boldsymbol{e}_2, \ldots, \boldsymbol{e}_N]$ is the $N\times(N-1)$ noise subspace composed of eigenvectors corresponding to the smaller eigenvalues.

The space spanned by the eigenvector corresponding to the large eigenvalue of the covariance matrix is the same as the space spanned by the steering vector of the incident signal with error, which is expressed as $\mathrm{span}\{\boldsymbol{e}_1\} = \mathrm{span}\{\Gamma\tilde{\mathbf{A}}\}$. We replace $a_i(\tilde{\theta}, \tilde{l})$ with $\tilde{a}_i$ $(-M \le i \le M)$. There is a parameter $w_{as}$ that satisfies the relationship of $w_{as}\boldsymbol{e}_1 = \Gamma\tilde{\mathbf{A}}$, and its detailed expression is as follows:

$$w_{as}\begin{bmatrix} e_{1,1} \\ \vdots \\ e_{1,n} \\ \vdots \\ e_{1,N} \end{bmatrix} = \begin{bmatrix} \Gamma_{-M}\widetilde{a}_{-M} \\ \vdots \\ \Gamma_0\widetilde{a}_0 \\ \vdots \\ \Gamma_M\widetilde{a}_M \end{bmatrix}. \tag{13}$$

The steering vector $\tilde{a}_0$ and the gain–phase error factor $\Gamma_0$ of the reference element are both 1. According to the reference array element, we obtain the detailed expression of the parameter $w_{as}$ and the gain–phase error factor $\widehat{\Gamma}_i$ of each array element as follows:

$$w_{as} = \frac{1}{e_{1,M+1}}, \tag{14}$$

$$\widehat{\Gamma}_i = \frac{w_{as}e_{1,n}}{\widetilde{a}_i},\ i = n-(M+1). \tag{15}$$

*Note.* In this section, the AS method is used to estimate the gain–phase error. However, the precondition of this method is that the actual position of AS is the same as the theoretical position and there is no error. If there is an error in the position of AS, the gain–phase error estimation results are inaccurate. In this paper, the actual position of AS is assumed to be the same as the theoretical position to avoid inaccurate estimation of the gain–phase error.

*3.2. Estimation of Source Steering Vector.* Based on the idea of space–time processing method, we delay the received data of each array element channel twice, and the delay time is $\Delta t$. The received data after the $i$-th time shift is represented as follows:

$$\boldsymbol{X}_{\Delta t,i} = \widehat{\boldsymbol{A}}\boldsymbol{\Psi}_{\Delta t,i}\boldsymbol{S} + \boldsymbol{N}_{\Delta t,i}, \tag{16}$$

where $\boldsymbol{\Psi}_{\Delta t,i} = \mathrm{diag}(e^{j2\pi f_1 i\Delta t}, \ldots, e^{j2\pi f_Q i\Delta t})$ is a $Q\times Q$ diagonal matrix related only to signal frequency and sampling interval. $\boldsymbol{N}_{\Delta t,i}$ is a $N\times K$ noise matrix.

We reconstruct the time-shift data of each order into a new $3N \times K$ data set, which is expressed as follows:

$$\boldsymbol{Z} = \begin{bmatrix} \boldsymbol{X}_{\Delta t,0} \\ \boldsymbol{X}_{\Delta t,1} \\ \boldsymbol{X}_{\Delta t,2} \end{bmatrix} = \begin{bmatrix} \widehat{\boldsymbol{A}}\boldsymbol{\Psi}_{\Delta t,0} \\ \widehat{\boldsymbol{A}}\boldsymbol{\Psi}_{\Delta t,1} \\ \widehat{\boldsymbol{A}}\boldsymbol{\Psi}_{\Delta t,2} \end{bmatrix} \boldsymbol{S} + \begin{bmatrix} \boldsymbol{N}_{\Delta t,0} \\ \boldsymbol{N}_{\Delta t,1} \\ \boldsymbol{N}_{\Delta t,2} \end{bmatrix} = \breve{\boldsymbol{A}}\,\boldsymbol{S} + \breve{\boldsymbol{N}}, \quad (17)$$

where $\boldsymbol{\Psi}_{\Delta t,0}$ is an $Q \times Q$ identity matrix. Two new data matrices $\boldsymbol{Z}_1 = \boldsymbol{J}_1\boldsymbol{Z}$ and $\boldsymbol{Z}_2 = \boldsymbol{J}_2\boldsymbol{Z}$ are extracted from the new data set, where $\boldsymbol{J}_1 = [\boldsymbol{I}_{2N},\ \boldsymbol{O}_{2N\times N}]$ and $\boldsymbol{J}_2 = [\boldsymbol{O}_{2N\times N},\ \boldsymbol{I}_{2N}]$. It is easy to prove that the array flow pattern matrix between the two data sets $\boldsymbol{Z}_1$ and $\boldsymbol{Z}_2$ satisfies $\breve{\boldsymbol{A}}_2 = \breve{\boldsymbol{A}}_1\boldsymbol{\Psi}_{\Delta t,1}$. The EVD of the covariance data matrix $\boldsymbol{Z}$ of the data matrix $\boldsymbol{R}_z = E[\boldsymbol{Z}\boldsymbol{Z}^H]$ is expressed as follows:

$$\boldsymbol{R}_z = \boldsymbol{U}_{ZS}\Lambda_S\boldsymbol{U}_{ZS}^H + \boldsymbol{U}_{ZN}\Lambda_N\boldsymbol{U}_{ZN}^H, \quad (18)$$

where $\Lambda_S = \mathrm{diag}\{\lambda_1, \ldots, \lambda_Q\}(\lambda_1 \geq \lambda_2 \geq \cdots \geq \lambda_Q)$ is a $Q \times Q$ diagonal matrix consisting of $Q$ larger eigenvalues, and $\Lambda_N = \mathrm{diag}\{\lambda_{Q+1}, \ldots, \lambda_{2N}\}(\lambda_{Q+1} = \lambda_{Q+2} = \cdots = \lambda_{2N} = \sigma_n^2)$ is a $(2N-Q)\times(2N-Q)$ diagonal matrix consisting of $(2N-Q)$ smaller eigenvalues. $\boldsymbol{U}_{ZS}$ represents the signal subspace composed of eigenvectors corresponding to $Q$ larger eigenvalues, and $\boldsymbol{U}_{ZN}$ represents the noise subspace composed of eigenvectors corresponding to $(2N-Q)$ smaller eigenvalues. $\boldsymbol{U}_{ZS}$ and $\breve{\boldsymbol{A}}$ have the same expansion subspace, that is $\mathrm{span}\{\boldsymbol{U}_{ZS}\} = \mathrm{span}\{\breve{\boldsymbol{A}}\}$. There exists a vector $\boldsymbol{T}$ such that $\boldsymbol{U}_{ZS}$ and $\breve{\boldsymbol{A}}$ satisfy

$$\boldsymbol{U}_{ZS} = \breve{\boldsymbol{A}}\,\boldsymbol{T}. \quad (19)$$

Since the relationship between $\boldsymbol{Z}_1, \boldsymbol{Z}_2$ and $\boldsymbol{Z}$, the steering vectors contained in $\boldsymbol{Z}_1$ and $\boldsymbol{Z}_2$ have the same spanning subspace with the first $2N$ rows and the last $2N$ rows of $\boldsymbol{Z}$, which are expressed as $\boldsymbol{U}_{ZS1} = \breve{\boldsymbol{A}}_1\boldsymbol{T}$ and $\boldsymbol{U}_{ZS2} = \breve{\boldsymbol{A}}_1\boldsymbol{\Psi}_{\Delta t,1}\boldsymbol{T}$. $\breve{\boldsymbol{A}}_1$ and $\breve{\boldsymbol{A}}_2$, respectively, represent the received data steering vectors for $\boldsymbol{Z}_1$ and $\boldsymbol{Z}_2$. $\boldsymbol{U}_{ZS2} = \boldsymbol{U}_{ZS1}\boldsymbol{T}^{-1}\boldsymbol{\Psi}_{\Delta t,1}\boldsymbol{T}$ can be obtained and $\boldsymbol{\Phi}$ is defined as $\boldsymbol{T}^{-1}\boldsymbol{\Psi}_{\Delta t,1}\boldsymbol{T}$. $\widehat{\boldsymbol{A}}$ can be directly estimated by the above relationship. Due to the presence of noise, the signal subspaces corresponding to $\boldsymbol{Z}_1$ and $\boldsymbol{Z}_2$ have perturbations of $\Delta\boldsymbol{U}_{ZS1}$ and $\Delta\boldsymbol{U}_{ZS2}$, respectively. When LS-ESPRIT algorithm calculates the steering vector estimate, only orthogonal subspaces of $\boldsymbol{U}_{ZS1}$ or $\boldsymbol{U}_{ZS2}$ can be constructed. In order to minimize the square of the perturbation norm when the noise disturbs both $\boldsymbol{U}_{ZS1}$ and $\boldsymbol{U}_{ZS2}$, the TLS-ESPRIT algorithm is used to compute $\boldsymbol{T}$. We define two new matrices $\boldsymbol{U}_{ZS12} = [\boldsymbol{U}_{ZS1}|\boldsymbol{U}_{ZS2}]$and $\boldsymbol{F}$ to correct the noise in both $\boldsymbol{U}_{ZS1}$ and $\boldsymbol{U}_{ZS2}$, in which $\boldsymbol{U}_{ZS12}\boldsymbol{F} = 0$. $\boldsymbol{F}$ can be obtained from the eigen decomposition of $\boldsymbol{U}_{ZS12}^H\boldsymbol{U}_{ZS12}$, which is expressed as follows:

$$\boldsymbol{U}_{ZS12}^H\boldsymbol{U}_{ZS12} = \boldsymbol{E}\Lambda_{ZS12}\boldsymbol{E}^H, \quad (20)$$

where $\Lambda_{ZS12}$ is a diagonal matrix with eigenvalues and $\boldsymbol{E}$ is a matrix composed of its corresponding eigenvector, which is expressed as follows:

$$\boldsymbol{E} = \begin{bmatrix} \boldsymbol{E}_{11} & \boldsymbol{E}_{12} \\ \boldsymbol{E}_{21} & \boldsymbol{E}_{22} \end{bmatrix}, \quad (21)$$

where we define $\boldsymbol{E}_N = [\boldsymbol{E}_{12}^T\ \boldsymbol{E}_{22}^T]^T$with characteristic vectors of zero eigenvalues and $\boldsymbol{U}_{ZS12}\boldsymbol{F} = 0$ when $\boldsymbol{F} = \boldsymbol{E}_N$. We can get the following relationship.

$$\begin{aligned} \boldsymbol{U}_{ZS12}\boldsymbol{F} &= [\boldsymbol{J}_1\boldsymbol{U}_{ZS}|\boldsymbol{J}_2\boldsymbol{U}_{ZS}] \begin{bmatrix} \boldsymbol{E}_{12} \\ \boldsymbol{E}_{22} \end{bmatrix} \\ &= \boldsymbol{J}_1\boldsymbol{U}_{ZS}\boldsymbol{E}_{12} + \boldsymbol{J}_2\boldsymbol{U}_{ZS}\boldsymbol{E}_{22} \\ &= \breve{\boldsymbol{A}}_1\boldsymbol{T}\boldsymbol{E}_{12} + \breve{\boldsymbol{A}}_1\boldsymbol{\Psi}_{\Delta t,1}\boldsymbol{T}\boldsymbol{E}_{22}. \end{aligned} \quad (22)$$

Combining $\boldsymbol{U}_{ZS12}\boldsymbol{F} = 0$ with the above formula, $\boldsymbol{T}^{-1}\boldsymbol{\Psi}_{\Delta t,1}\boldsymbol{T} = -\boldsymbol{E}_{12}\boldsymbol{E}_{22}^{-1}$ can be obtained and $\widehat{\boldsymbol{\Phi}}_{\mathrm{TLS}} = -\boldsymbol{E}_{12}\boldsymbol{E}_{22}^{-1}$ can be defined. Since $\boldsymbol{\Psi}_{\Delta t,1}$ is a diagonal matrix, the eigenvector of $\widehat{\boldsymbol{\Phi}}_{\mathrm{TLS}}$ has the same expansion space as $\boldsymbol{T}^{-1}$, and the feature decomposition of $\widehat{\boldsymbol{\Phi}}_{\mathrm{TLS}}$ is expressed as follows:

$$\widehat{\boldsymbol{\Phi}}_{\mathrm{TLS}} = \boldsymbol{E}_{\mathrm{TLS}}\Lambda_{\mathrm{TLS}}\boldsymbol{E}_{\mathrm{TLS}}^H, \quad (23)$$

where $\boldsymbol{E}_{\mathrm{TLS}}$ is the eigenvector of $\widehat{\boldsymbol{\Phi}}_{\mathrm{TLS}}, \Lambda_{\mathrm{TLS}}$ is the feature of $\widehat{\boldsymbol{\Phi}}_{\mathrm{TLS}}$ and $\mathrm{span}\{\boldsymbol{T}^{-1}\} = \mathrm{span}\{\boldsymbol{E}_{\mathrm{TLS}}\}$, in which $\boldsymbol{T}^{-1}$ can be expressed as follows:

$$\widetilde{\boldsymbol{T}}^{-1} = \boldsymbol{E}_{\mathrm{TLS}} \cdot \boldsymbol{w}, \quad (24)$$

where $\boldsymbol{w} = [\boldsymbol{w}_{-M}^T, \ldots, \boldsymbol{w}_0^T, \ldots, \boldsymbol{w}_M^T]^T$ is a coefficient matrix, in which $\boldsymbol{w}_i = [w_{i,1}, \ldots, w_{i,Q}]$ and $w_{-M,q} = \cdots = w_{0,q} = \cdots = w_{-M,q}$.

Combined with Equation (24), $\breve{\boldsymbol{A}}_1 = \boldsymbol{U}_{ZS1}\boldsymbol{E}_{\mathrm{TLS}} \cdot \boldsymbol{w}$ can be obtained from $\boldsymbol{U}_{ZS1} = \breve{\boldsymbol{A}}_1\boldsymbol{T}$, and the first $N$ rows of $\breve{\boldsymbol{A}}_1$ are marked as $\widehat{\boldsymbol{A}}$, which is an estimate of $\widehat{\boldsymbol{A}}$. We denote the first $N$ rows $\boldsymbol{U}_{ZS1}\boldsymbol{E}_{\mathrm{TLS}}$ as $\hat{\boldsymbol{U}}_{\mathrm{TLS}} = [\boldsymbol{u}_{-M}^T, \ldots, \boldsymbol{u}_0^T, \ldots, \boldsymbol{u}_M^T]^T$, in which $\boldsymbol{u}_i = [u_{i,1}, \ldots, u_{i,Q}]$. Because the $a_0(\theta_q, L_q)$ in $\widehat{\boldsymbol{A}}$ is 1, we can get

$$w_{0,q} = \frac{1}{u_{0,q}}. \quad (25)$$

According to $\breve{\boldsymbol{A}}_1 = \boldsymbol{U}_{ZS1}\boldsymbol{E}_{TLS} \cdot \boldsymbol{w}$ and Equation (25), the estimated value of $\widehat{\boldsymbol{A}}$ can be obtained.

*3.3. Accurate Estimation of Source Location.* The AS method is used to obtain the estimated value of the gain–phase error matrix $\widehat{\Gamma}$ and the TLS-ESPRIT algorithm is used to obtain the estimated value of the steering vector $\breve{\boldsymbol{A}}_1$ containing the error. The accurate source steering vector can be constructed by $\widehat{\Gamma}$ and $\breve{\boldsymbol{A}}_1$. It is expressed as follows:

$$\overline{\boldsymbol{A}} = \widehat{\Gamma}^{-1}\breve{\boldsymbol{A}}_1, \tag{26}$$

where $\overline{\boldsymbol{A}}$ is the estimate of $\boldsymbol{A}$.

The magnitude and phase of the two elements adjacent to the reference element are used to realize the near-field source location. $|\rho_{-1}|$ and $|\rho_1|$ are denoted as $\widehat{\rho}_{-1}$ and $\widehat{\rho}_1$, respectively. According to the study of He et al. [27], $\widehat{\rho}_{-1}$ and $\widehat{\rho}_1$ with the $q$th source position $(\theta_q,\ L_q)$ coordinate relationship is expressed as follows:

$$\begin{cases} \dfrac{L_q}{\sqrt{L_q^2 + d_1^2 - 2L_q d_1 \sin\theta_q}} = \widehat{\rho}_{1,q} \\ \dfrac{L_q}{\sqrt{L_q^2 + d_{-1}^2 - 2L_q d_{-1} \sin\theta_q}} = \widehat{\rho}_{-1,q}. \end{cases} \tag{27}$$

The result in the above expression is an estimate of the angle and range of the source position, expressed as follows:

$$\begin{cases} \widehat{L}_q = \sqrt{\dfrac{d_1 d_{-1}(d_1 - d_{-1})\rho_{1,q}^2\rho_{-1,q}^2}{d_1\rho_{1,q}^2\rho_{-1,q}^2 - \rho_{1,q}^2\rho_{-1,q}^2 d_{-1} + \rho_{-1,q}^2 d_{-1}}} \\ \widehat{\theta}_q = \arcsin\left(\dfrac{\rho_{1,q}^2 d_1 + \widehat{L}_q^2\rho_{1,q}^2 - \widehat{L}_q^2}{\rho_{1,q}^2 2\widehat{L}_q d_1}\right), \end{cases} \tag{28}$$

where $\widehat{L}_q$ and $\widehat{\theta}_q$ are the solutions of the error-free magnitude formula, and the phase is used to further estimate the source position. It is shown in [27] and [28] that there is an uncertain phase factor between the phase difference generated by the distance difference and the phase of the steering vector. In this paper, the idea of accurate estimation in [27] is used. It is easy to get the phase difference estimate of $q$-th source received by two elements adjacent to the reference element, denoted as $\tilde{\varphi}_{-1,q}$ and $\tilde{\varphi}_{1,q}$, respectively. Once $\tilde{\varphi}_{-1,q}$ and $\tilde{\varphi}_{1,q}$ are determined, the two phase-dependent equations can be expressed as follows:

$$\begin{cases} L_q - \sqrt{L_q^2 + d_{-1}^2 - 2L_q d_{-1}\sin\theta_q} = \dfrac{\lambda\widetilde{\varphi}_{-1,q}}{2\pi} = B_{-1,q} \\ L_q - \sqrt{L_q^2 + d_1^2 - 2L_q d_1 \sin\theta_q} = \dfrac{\lambda\widetilde{\varphi}_{1,q}}{2\pi} = B_{1,q}. \end{cases} \tag{29}$$

The accurate estimation results of angle and range are expressed as follows:

$$\widetilde{L}_q = \frac{d_{-1}B_{1,q}^2 - d_1 B_{-1,q}^2 + d_1 d_{-1}^2 - d_{-1}d_1^2}{2d_{-1}B_1 - 2d_1 B_{-1}}, \tag{30}$$

$$\widetilde{\theta}_q = \arcsin\left(\frac{2\widetilde{L}_q B_1 - B_1^2 + d_1^2}{2\widetilde{L}_q d_1}\right). \tag{31}$$

## 4. Discussion and Performance Analysis

The performance of proposed algorithm is examined in terms of the computational complexity and the greatest number of resolvable sources. The performance of proposed algorithm for estimating the position of mixed sources is proven through derivation.

*4.1. Computational Complexity.* For the computational complexity of the proposed algorithm, we primarily address the data covariance matrix and EVD based on the time-shift method. The EVD is subdivided into the EVD of the AS data covariance matrix, the reconstructed data covariance matrix, and the TLS-ESPRIT method.

The gain–phase error multiplication method focuses primarily on the generation of the AS covariance matrix $\tilde{\boldsymbol{R}}$ and the EVD of $\tilde{\boldsymbol{R}}$ and its computational cost is defined as $O(N^3 + \mathrm{K}N^2)$. The computational complexity in the building of the new data matrix after time shift is expressed as $O((3N)^2\mathrm{K})$ and the computational complexity in the EVD of the covariance matrix $\boldsymbol{R}_Z$ concerning the new data is expressed as $O((3N)^3)$. The computational difficulty of building matrix $\boldsymbol{U}_{ZS12}^H\boldsymbol{U}_{ZS12}$ in the TLS-ESPRIT approach is $O((2N)^2\mathrm{2K})$, while the computational complexity of $\boldsymbol{U}_{ZS12}^H\boldsymbol{U}_{ZS12}$ eigenvalue decomposition is $O((2N)^3)$. In addition to the computational complexity of the preceding processes, the computational complexity of predicting the exact source guiding vector without error is denoted by $O(N^2Q)$. In summary, the computational complexity of the suggested method is given as $O(36N^3 + 15\mathrm{K}N^2 + N^2Q)$. The results of complexity comparison with existing algorithms are shown in Table 1. The computational complexity of the proposed algorithm is higher than that of some existing algorithms, but it is better than that of the algorithm based on special fourth-order cumulant or spatial spectrum.

*4.2. Maximum Number of Resolvable Sources.* The majority of gain–phase error-based near-field source localization techniques, such as [20, 21, 24], estimate the location of RNF source by building a unique fourth-order cumulant $\boldsymbol{R}_{\mathrm{com}}(N \times N)$. According to the subspace theory [29, 30], the EVD of data matrix has at least one eigenvector that corresponds to the noise subspace. As a result, $N-1$ is the maximum number of sources that can be estimated using the aforementioned techniques, which is fewer than the minimum number of rows and columns in the data covariance matrix. In the investigation, the time-shift approach is used to create a new $3N \times K$-dimensional receiving data matrix $\boldsymbol{Z}$, thus increasing the degree of freedom of the algorithm. Full rank is a necessary condition for the TLS-ESPRIT approach in this research, hence the maximum estimated source number of the suggested algorithm is $2N-1$. In the proposed method, only the reference element receives correct data, and all other elements receive data that are connected to the signal-to-noise ratios (SNRs) of the AS and the source. The suggested method is unable to recognize and find many sources if the aforementioned two SNRs are low. The next part examines the unique

Table 1: The performance comparison between the algorithm and the existing results.

| | Array model | Computational complexity | Maximum number of resolvable sources |
|---|---|---|---|
| [15] | Fresnel model | $O(9N^2\mathrm{K}+9(M+N)^2\mathrm{K}+\frac{4(QN^3+(N+M)^3)}{3}+20001N^2)$ | $N-1$ |
| [20] | Fresnel model | $O(12\cdot 9(6N)^2\mathrm{K}+\frac{8(36N)^3}{3}+20Q^2(6N)+(6N)^2\mathrm{K}+\frac{4(6N)^3}{3})$ | $N-1$ |
| [23] | Exact model | $O(3N^2\mathrm{K}^2+Q^2(3N+Q)+6NQ^2)$ | $N-1$ |
| [24] | Exact model | $O((6N^2+8N+3)\mathrm{K}+54N^3+2Q^3)$ | $N-1$ |
| The proposed algorithm | Exact model | $O(36N^3+15\mathrm{K}N^2+N^2Q)$ | $2N-1$ |

circumstance. It can be seen from Table 1 that under the condition of amplitude phase error, the maximum estimable source number of the proposed algorithm is much larger than that of other existing algorithms.

*4.3. Applicability to Locate Mixed Sources.* We outline the theoretical justification for the proposed method to handle RNF sources localization in Section 3. But in reality, the source in environment is a combination of RNF and RFF sources. The expansion of the proposed method for mixed source location is quite important. The application of the suggested method to the location of mixed sources is mostly introduced in this part.

By contrasting the source position with the RNF and RFF boundaries, the source location is identified. Assume that the $g$th source is in the position $(\theta_g,\ L_g)$, where it is when $L_g \le 2D^2/\lambda$ is, and when $L_g > 2D^2/\lambda$ is, RNF and RFF, respectively. In this paper, the distance between the source and the $i$th array element is defined as follows:

$$l_{i,g}=\sqrt{\left(L_g\sin\theta_g-d_i\right)^2+\left(L_g\cos\theta_g\right)^2}, \tag{32}$$

and the Taylor second-order expansion of above formula is as follows:

$$l_{i,g}\approx L_g-d_i\sin\theta_g+\frac{d_i^2\cos^2\theta_g}{2L_g}+o\left(\frac{d_i}{L_g}\right), \tag{33}$$

where $o(d_i/L_g)$ is a polynomial of higher order in $d_i/L_g$. The higher order is negligible when the $L_g$ of RFF approaches infinity.

The amplitude and phase factor between the $i$th array element and the $g$th source is stated as $a_i(\theta_g,\ L_g)=\tilde{\eta}_{i,g}e^{j\tilde{\varphi}_{i,g}}$ using Equation (2) and the second-order Taylor approximation of the distance, where $\tilde{\eta}_{i,g}$ and $\tilde{\varphi}_{i,g}$ are written as follows:

$$\widetilde{\eta}_{i,g}=\frac{1}{1-\frac{d_i}{L_g}\sin\theta_g+\frac{d_i^2}{L_g^2}\frac{\cos^2\theta_g}{2}}, \tag{34}$$

and

$$\widetilde{\varphi}_{i,g}=-\frac{2\pi}{\lambda}\left(d_i\sin\theta_g-\frac{d_i^2\cos^2\theta_g}{2L_g}\right), \tag{35}$$

where since $L_g\to\infty$, so $d_i/L_g\to 0$ and $d_i^2/L_g\to 0$. The approximate amplitude factor is expressed as $\tilde{\eta}_{i,g}=1$, and the phase factor is expressed as $\tilde{\varphi}_{i,g}=-2\pi d_i\sin\theta_g/\lambda$. The simplified amplitude and phase factor is expressed as follows:

$$a_F\left(\theta_g,\ L_g\right)=e^{-j\frac{2\pi}{\lambda}d_i\sin\theta_g}. \tag{36}$$

*Note*. After derivation, the RFF steering vector expression in the current results is an expression of Equation (2) in specific circumstances, making the simplified form of Equation (2) under RFF the same as that of the results. The steering vectors for the RFF and RNF sources in this study are both represented by Equation (2).

Assume that the environment contains G narrowband and incoherent sources, where Q is the number of RNF sources and G-Q is the number of RFF sources. The array receiving data is expressed as follows:

$$\begin{aligned}\widehat{\boldsymbol{X}}(t)&=\sum_{q=1}^{Q}\widehat{\boldsymbol{a}}\left(\theta_q,\ L_q\right)s_q(t)+\sum_{g=Q+1}^{G}\widehat{\boldsymbol{a}}\left(\theta_g,\ L_g\right)s_g(t)+\boldsymbol{n}(t)\\&=\widehat{\boldsymbol{A}}_N\boldsymbol{S}_N(t)+\widehat{\boldsymbol{A}}_F\boldsymbol{S}_F(t)+\boldsymbol{N}(t)\\&=\Gamma(\boldsymbol{A}_N\boldsymbol{S}_N(t)+\boldsymbol{A}_F\boldsymbol{S}_F(t))+\boldsymbol{N}(t),\end{aligned} \tag{37}$$

where $\widehat{\boldsymbol{A}}_N$ and $\widehat{\boldsymbol{A}}_F$ represent the array manifold vectors of RNF source and RFF source with gain–phase errors, respectively. $\widehat{\boldsymbol{a}}(\theta_q,\ L_q)$ and $\widehat{\boldsymbol{a}}(\theta_g,\ L_g)$ represent the steering vectors of RNF source and RFF source with gain–phase errors, respectively, where $(\theta_q,\ L_q)$ is the position coordinate of RNF source, $(\theta_g,\ L_g)$ is the position coordinate of RFF source and $L_p\gg L_g$.

The estimate results of the location of the mixed source are obtained using the TLS-ESPRIT concept and the time shift of the mixed source in accordance with the source location technique in Section 3 since the source model under RNF and RFF in this work is described in the same way. In mixed source location results, the Fresnel–Fraunhofer border is employed to separate RFF and RNF sources. The source is categorized as an RNF source if the distance estimate result is smaller than the boundary value and an RFF source in all other cases.

*Remark*. The suggested approach must guarantee complete rank, hence $G\le 2N-1$ is used for the eigenvector of

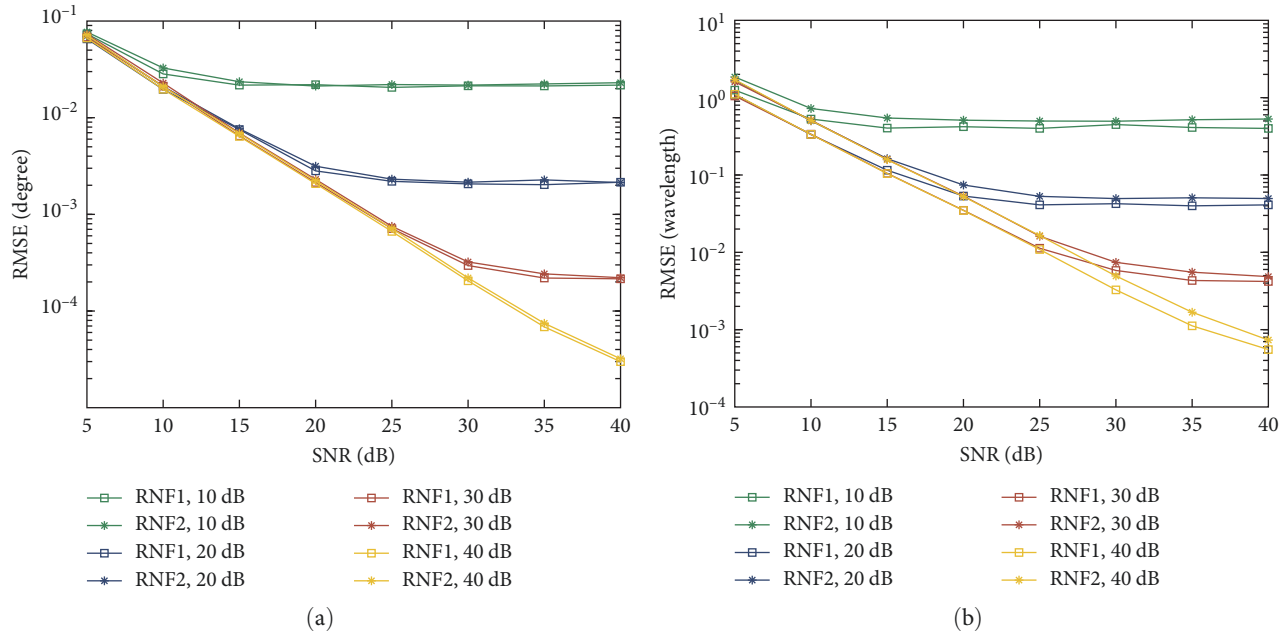


FIGURE 2: The variation curve of RMSE of source location results with the AS SNR. (a) RMSE of angle estimation. (b) RMSE of range estimation.

mixed source covariance data matrix. Furthermore, the distance difference between an RFF source and various elements is smaller than that between an RNF source and various elements and can essentially not be recorded because the RFF source is located at a much greater distance than an RNF source. As a result, in the RFF origin location, only the assessment of the incoming wave direction of source is considered.

## 5. Simulation and Analysis

This section examines the near-field source positioning, error analysis of the positioning findings, neighboring source positioning, multisource positioning, and mixed source positioning aspects of the positioning performance of the proposed method. Unless there are any unique circumstances, the following conditions often govern experiments. The experiment employs a nonuniform linear array of nine elements, with the precise location of elements in this paper being $[-2.5, -1.8, -1.2, -0.7, 0, 0.9, 1.5, 2.3, 3]\lambda$. The RNF range of array is $[7.99, 60.5]\lambda$, and the $60.5\lambda$ marks the border between the Fresnel zone and the Fraunhofer zone. The gain–phase error factor of all other position elements aside from the reference element is $0.42 \times (\text{randn}(1,1) + j \times \text{randn}(1,1)) + 1$. The AS is at $(10°, 16\lambda)$ and has an SNR of 20 dB. The SNR for all sources is 20 dB, and the source has 1,000 snapshots. There are 500 statistically independent Monte Carlo trials performed on all the experimental data. The experiments shown were all carried out on Intel(R) Core (TM) i7-12,700H, 12 core, Windows 11(64) environment by downloading MATLAB software.

*5.1. The Influence of AS.* This experiment simulates the impact of ASs with various SNRs on the positioning performance of algorithm. The source position estimate is realized in four scenarios when the SNR of the two RNF sources is 10, 20, 30, and 40 dB, respectively, considering the variable range of the SNR of AS (AS SNR) as being [5 40] dB. The estimated findings' root-mean-square error (RMSE), is a parameter used to gauge algorithm performance. The source estimation results' RMSE is written as follows:

$$\begin{cases} \text{RMSE}_\theta = \sqrt{\dfrac{1}{KM_m} \sum_{i=1}^{K} \sum_{i=1}^{M_m} \left(\widehat{\theta} - \theta\right)^2} \\ \text{RMSE}_L = \dfrac{1}{\lambda} \sqrt{\dfrac{1}{KM_m} \sum_{i=1}^{K} \sum_{i=1}^{M_m} \left(\widehat{L} - L\right)^2}, \end{cases} \tag{38}$$

where $M_m$ is the number of independent trials, $(\widehat{\theta}, \widehat{L})$ and $(\theta, L)$ are the estimated and true values of the source location, respectively.

The experimental findings are depicted in Figure 2, where (a) represents the change in RMSE of the results of angle estimation with the AS SNR and (b) represents the change in RMSE of the results of range estimation with the AS SNR. The experimental results demonstrate a relationship between the AS SNR and the source SNR and the error of source location parameter estimate. With an increase in the SNR of the AS, the RMSE of the source location estimation findings does not always go down. It is limited by the SNR of source, thus when it is dropped to a specific amount, the RMSE of the source location estimation results remains unchanged. To summarize, if the AS SNR is high, it can effectively reduce the error of the source position estimation result with high SNR but has little effect on the source position estimation result with low SNR.

In addition, we consider the positioning performance of the algorithm when there are errors in the AS position. The

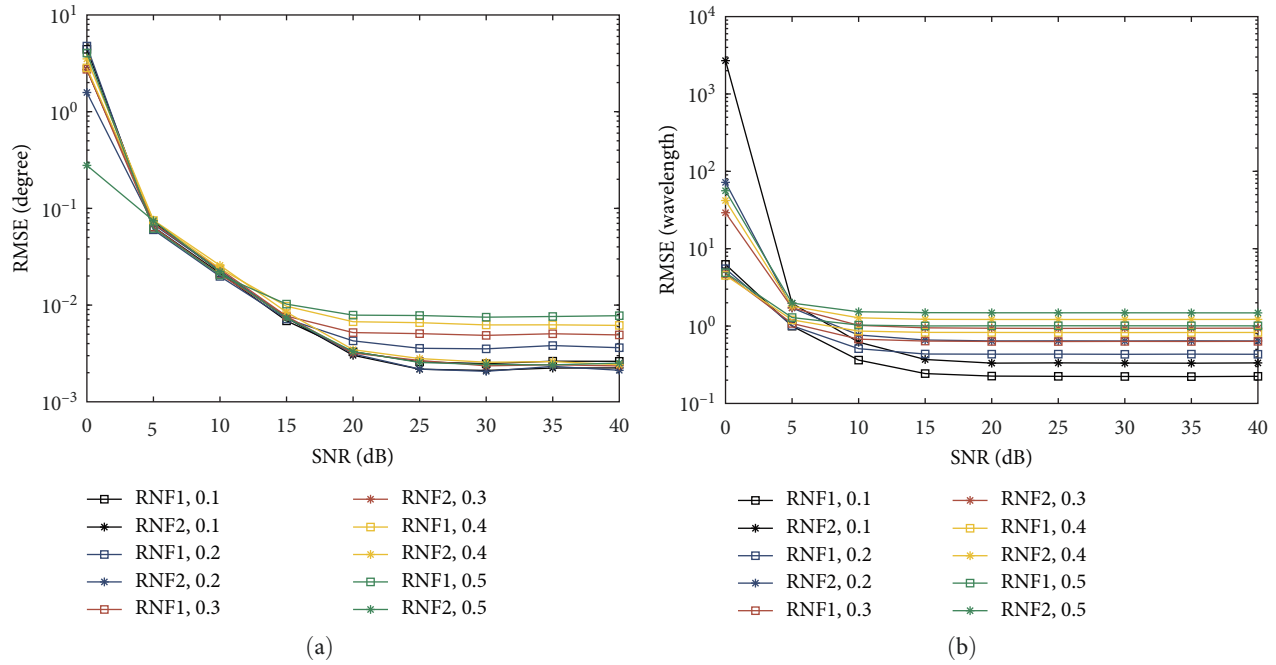


Figure 3: The variation curve of RMSE of source location results with the AS angle. (a) RMSE of angle estimation. (b) RMSE of range estimation.

experimental results are shown in Figures 3 and 4. Figure 3 is the RMSE curve of source location estimation results when there is different bias in AS angle, and Figure 4 is the RMSE curve of source location estimation results when there is different bias in AS range. In Figures 3(a) and 3(b), where there is an AS angle error, we consider that the angle error is up to 0.5°. In Figures 4(a) and 4(b) where there is an error in the AS range, we consider the maximum range error to be $0.5\lambda$. The experimental results show that when the angle error or range error of AS is larger, the estimation error of source position estimation is larger. Under the condition that SNR is greater than 10 dB, the estimation results of source position parameters with AS error have relatively large error, but the source location can still be realized.

*5.2. RNF Source Localization Results.* Assume that the experimental environment has two incoherent RNF sources at $(-15°, 15\lambda)$ and $(20°, 18\lambda)$. The estimation result of 500 independent trials of the two RNF sources is shown in Figure 5, where (a) is the angle estimation result and (b) is the range estimation result. The results of RNF source angle estimation reveal that the proposed method can accurately estimate the direction of the signal source in the presence of gain–phase error. In 500 experiments, there is an inaccuracy between the estimated source distance parameter and the actual position of the source, but the difference is modest and within an acceptable range. The simulation results show that the proposed method can estimate the RNF source with gain–phase error accurately.

*5.3. Performance of RNF Source DOA Estimation.* The RMSE trend of the source location estimate results is examined in this subsection from the perspectives of SNR and snapshots, where snapshots are made up of low and high snapshots. The proposed algorithm is compared to the methods presented in [15] (TS-MUSIC in abbreviation) and [24] (PCA in abbreviation), as well as Cramér-Rao Bound (CRB), which gives a lower bound for parameter estimates. The CRB verification and derivation with gain–phase errors under an accurate signal model have been completed in [24]. The RMSE of the source location estimation results with the SNR curve is shown in Figure 6, and the curve with the number of snapshots is shown in Figures 7 and 8, where Figure 5 represents the source location estimation result with high snapshots (100–1,000) and Figure 6 represents the source location estimation result with low snapshots (10–100).

Figure 6 depicts the change curve of the source angle estimation result (a) and the change curve of the source range estimation result (b). The TS-MUSIC and PCA algorithms are incapable of achieving source localization, and the source location estimate results still have significant errors as the SNR increases. However, the proposed method can estimate the source position, and the estimation results have decreasing errors as the SNR increases. When the SNR is less than 5 dB, the proposed method produces inaccurate source localization findings. When SNR exceeds 5 dB, the inaccuracy of the source position estimate result of proposed algorithm decreases and remains constant throughout the SNR range (20–40)dB.

In Figures 7 and 8, the source location estimation results of the TS-MUSIC and PCA algorithms exhibit significant inaccuracies and are unable to determine the source location, regardless of the value of the number of snapshots. The source position can be accurately predicted by the proposed method, and the source position prediction result has a minimal error. When the number of snapshots is small in

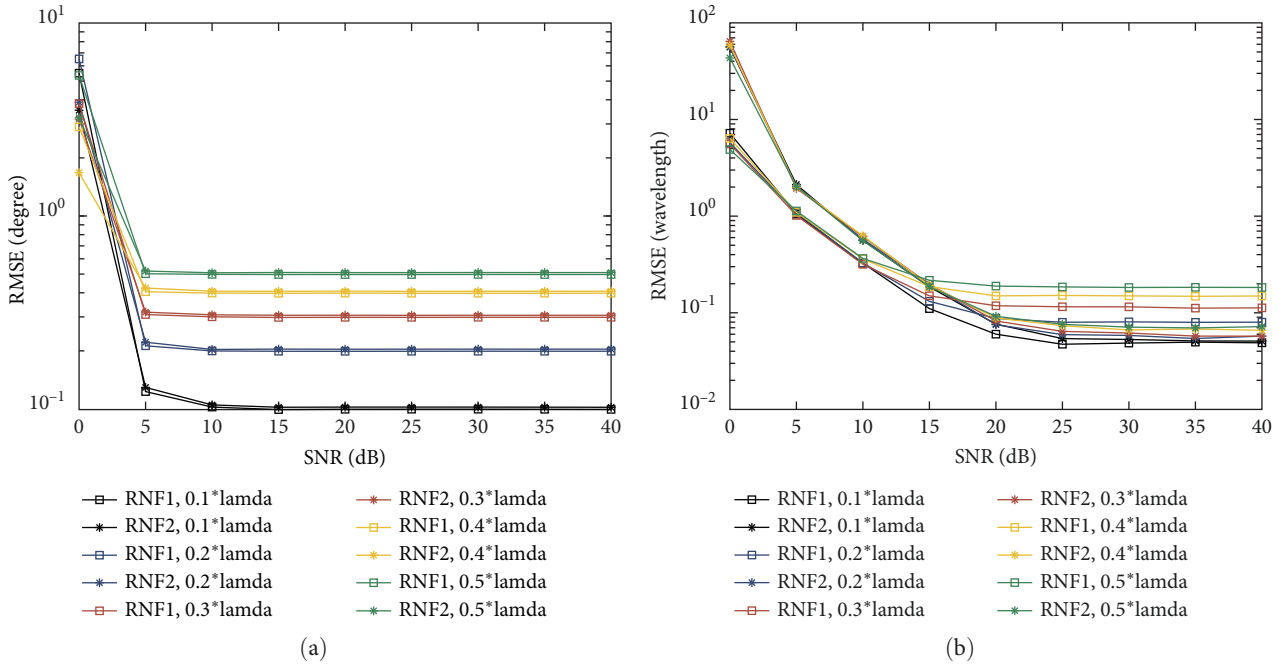


Figure 4: The variation curve of RMSE of source location results with the AS range. (a) RMSE of angle estimation. (b) RMSE of range estimation 5.2 RNF source localization results.

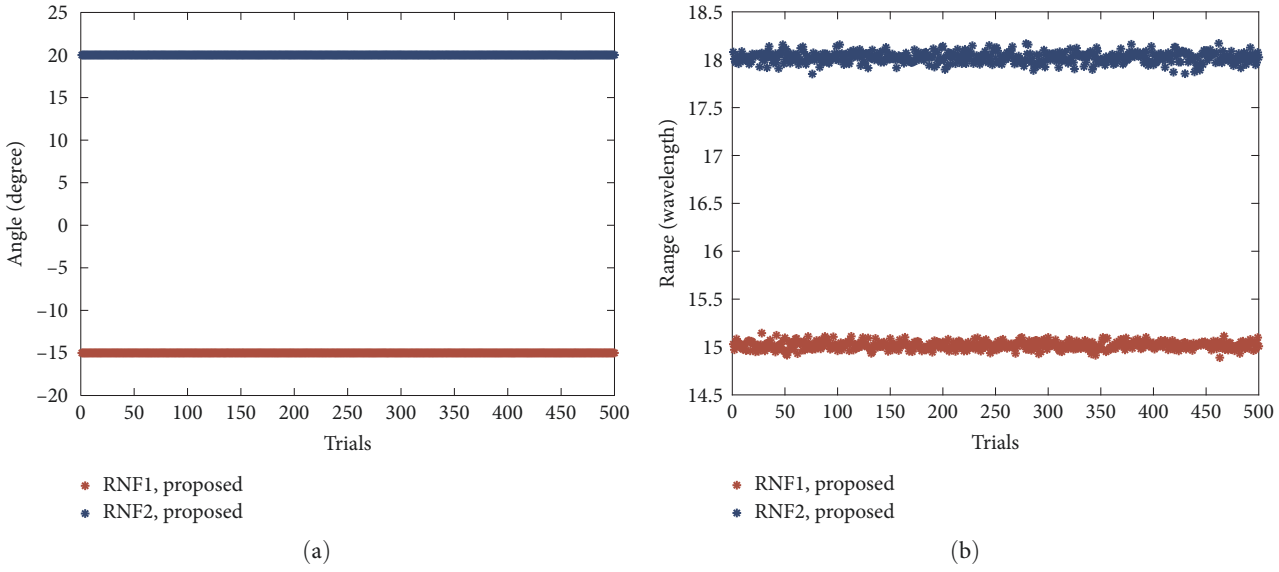


Figure 5: The position estimation results of 500 trials of two RNF sources. (a) Angle estimation results. (b) Range estimation results.

Figures 8(a) and 8(b), the error of source location parameter estimation decreases with the increase of the number of snapshots. However, when the number of snapshots is high in Figures 7(a) and 7(b), the change of the number of snapshots has little effect on the error of the source position parameter estimation results. In a nutshell since the PCA algorithm determines the near-field source location based on the calibrated element receiving data, the processed data is still perfect data without error, which is challenging to achieve in practice, even for all elements with gain–phase errors (aside from reference elements). In comparison to existing techniques, the proposed method can efficiently accomplish accurate estimate of RNF source location parameters.

*5.4. Adjacent RNF Source Location Performance.* This section uses two examples of adjacent angles of the same range and adjacent ranges of the same angle to demonstrate the localization performance of the s proposed algorithm for adjacent RNF sources. $(15.03°, 15\lambda)$ and $(15.04°, 15\lambda)$ (in the same range) and $(15°, 15\lambda)$ and $(15°, 14.8\lambda)$ (at the same angle) are assumed to be the source sites in the two examples,

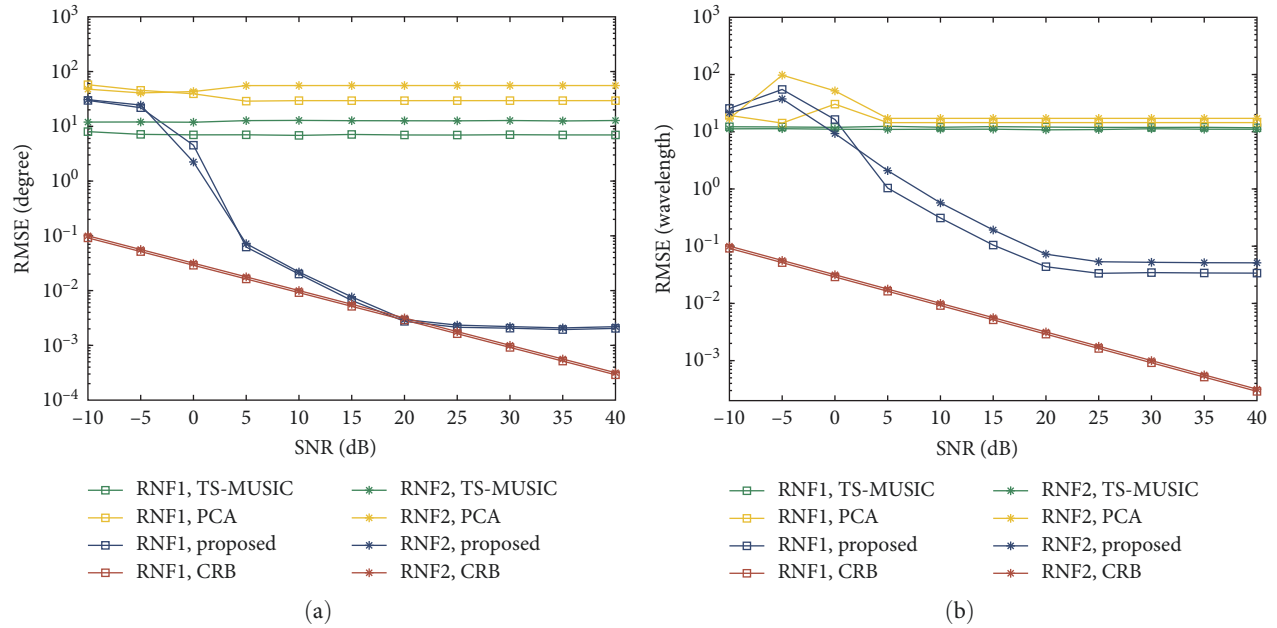


Figure 6: The variation curve of RMSE of RNF sources location results with the SNR. (a) RMSE of angle estimation. (b) RMSE of range estimation.

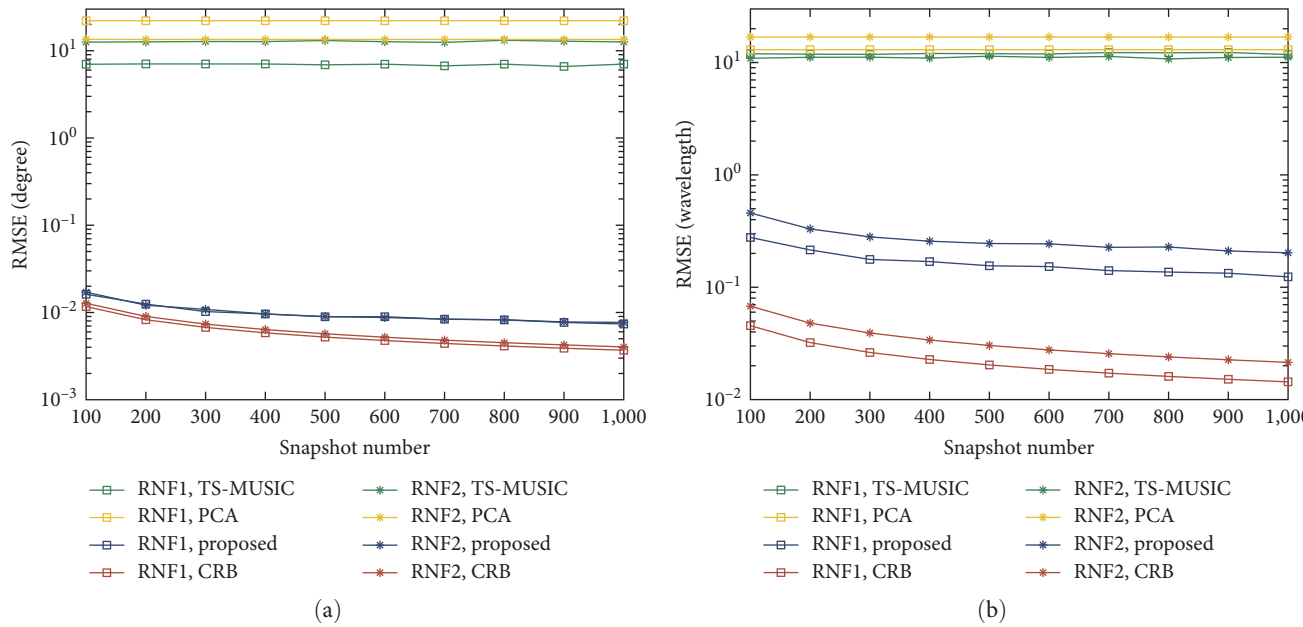


Figure 7: The variation curve of RMSE of RNF sources location results with the snapshot. (a) RMSE of angle estimation. (b) RMSE of range estimation.

respectively. The results of adjacent source location in the two situations and the likelihood that sources would be successfully resolved by the proposed algorithm are depicted in Figures 9 and 10.

Figure 9(a) shows the location results of two adjacent sources with the same range, while Figure 9(b) shows the location results of two adjacent sources with the same Angle. The experimental results show that the proposed algorithm can accurately locate adjacent sources in both cases. Additionally, the location results of adjacent RNF sources in both scenarios are very close to the real position of source. As shown in Figures 10(a) and 10(b), the proposed algorithm has a higher probability of successfully locating two adjacent RNF sources as SNR increases. When the SNR of source reaches more than 20 dB, the proposed algorithm has a higher probability of successfully locating two adjacent RNF sources under two conditions. In conclusion, the proposed method can find adjacent RNF sources reliably and

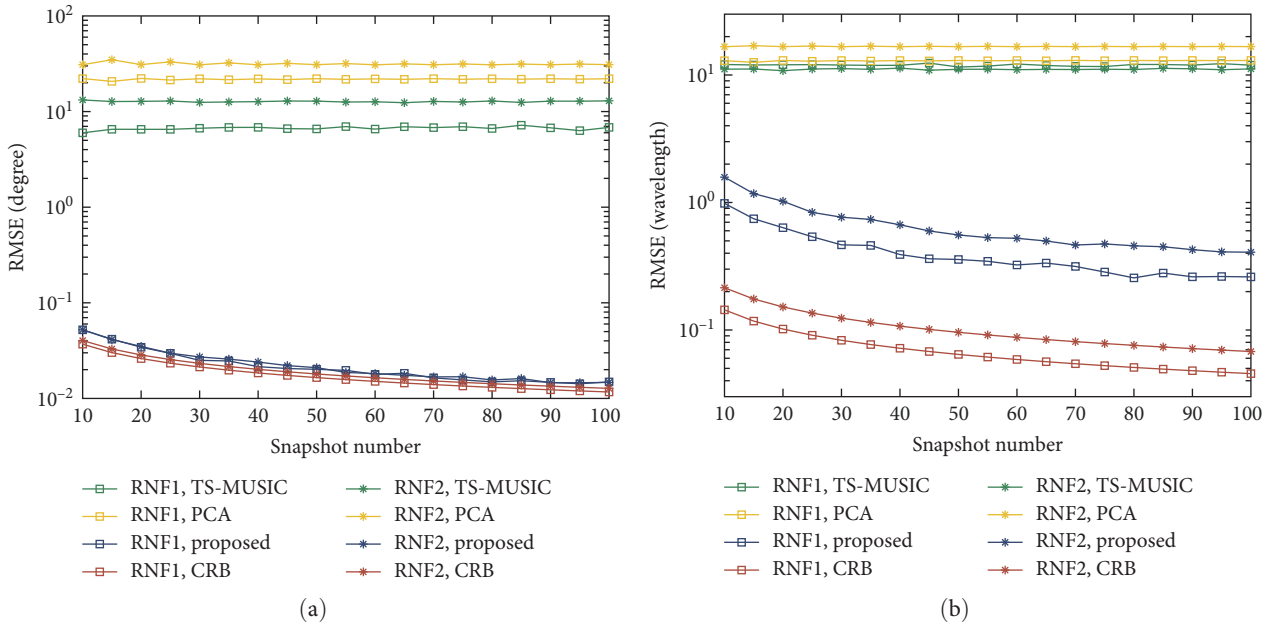


FIGURE 8: The variation curve of RMSE of RNF sources location results with the low snapshot. (a) RMSE of angle estimation. (b) RMSE of range estimation.

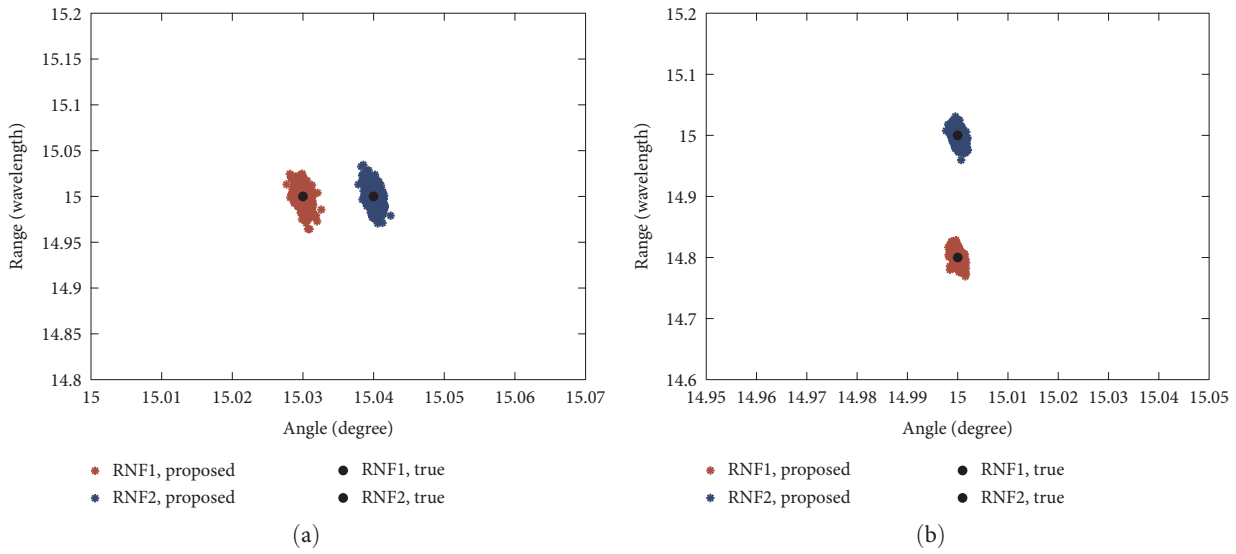


FIGURE 9: The 500 experimental results of adjacent RNF sources. (a) Same range. (b) Same angle.

has a high-resolution probability when the source has a high SNR.

*5.5. Location Performance of Multiple Sources.* To demonstrate that the proposed method has greater array freedom, we test its localization performance for many sources under diverse array elements. The two sets of experiments are expected to employ an array of five elements and nine elements, respectively, to estimate the positions of nine incoherent sources and 17 incoherent sources. The element distribution position of the array antenna composed of five elements is $[-1.2, -0.7, 0, 0.9, 1.5]\lambda$. Tables 2 and 3 give the mean and true values of the 500 experimental estimation results of the proposed algorithm for multiple RNF sources under different array antennas.

As shown in Figure 11, the proposed method performs 500 experimental estimations of multiple RNF source locations using various array antennas, in which the Figure 11(a) demonstrates the multisource location results under five arrays and Figure 11(b) demonstrates the multisource location results under nine arrays. The real position of the RNF source is shown by the black hollow circle in the figure, while the predicted position of the RNF source is indicated by different colors. The figure shows that the proposed method

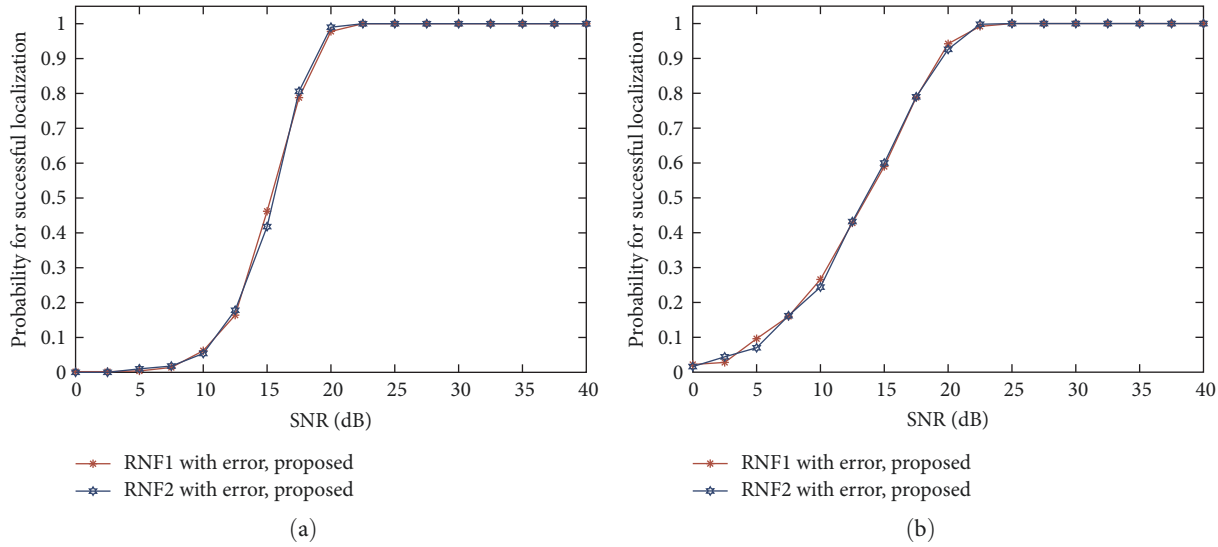


Figure 10: Probability of successful location of adjacent RNF sources versus SNR. (a) Same range. (b) Same angle.

Table 2: Source real location and estimated position (5-element case).

| Source number | Actual position | Position estimation mean |
|---|---|---|
| Source 1 | $(-15°, 12.5\lambda)$ | $(-15.0019°, 12.5179\lambda)$ |
| Source 2 | $(10°, 9\lambda)$ | $(10.0020°, 8.9944\lambda)$ |
| Source 3 | $(5°, 13\lambda)$ | $(4.9985°, 12.9900\lambda)$ |
| Source 4 | $(-25°, 7\lambda)$ | $(-25.0023°, 6.9975\lambda)$ |
| Source 5 | $(-5°, 6\lambda)$ | $(-5.0117°, 5.9988\lambda)$ |
| Source 6 | $(15°, 3.5\lambda)$ | $(15.0037°, 3.4985\lambda)$ |
| Source 7 | $(30°, 5.5\lambda)$ | $(30.0003°, 5.4997\lambda)$ |
| Source 8 | $(27.5°, 9.7\lambda)$ | $(27.4999°, 9.6999\lambda)$ |
| Source 9 | $(-6.5°, 4.3\lambda)$ | $(-6.4995°, 4.2992\lambda)$ |

Table 3: Source real location and estimated position (9-element case).

| Source number | Actual position | Position estimation mean |
|---|---|---|
| Source 1 | $(-15°, 12.5\lambda)$ | $(-14.9998°, 12.4964\lambda)$ |
| Source 2 | $(10°, 9\lambda)$ | $(10.0001°, 8.9984\lambda)$ |
| Source 3 | $(5°, 23\lambda)$ | $(5.0001°, 22.9929\lambda)$ |
| Source 4 | $(-25°, 17\lambda)$ | $(-25.0015°, 17.0136\lambda)$ |
| Source 5 | $(-5°, 6\lambda)$ | $(-4.9999°, 5.9994\lambda)$ |
| Source 6 | $(15°, 13.5\lambda)$ | $(14.9993°, 13.5073\lambda)$ |
| Source 7 | $(30°, 15.5\lambda)$ | $(30.0001°, 15.4983\lambda)$ |
| Source 8 | $(27.5°, 21\lambda)$ | $(27.4999°, 20.9976\lambda)$ |
| Source 9 | $(-6.5°, 8\lambda)$ | $(-6.4999°, 8.0000\lambda)$ |
| Source 10 | $(-30°, 18.5\lambda)$ | $(-29.9999°, 18.4966\lambda)$ |
| Source 11 | $(-20°, 14\lambda)$ | $(-20.0001°, 14.0031\lambda)$ |
| Source 12 | $(20°, 14.5\lambda)$ | $(20.0003°, 14.4961\lambda)$ |
| Source 13 | $(33°, 16.5\lambda)$ | $(33.0001°, 16.4980\lambda)$ |
| Source 14 | $(17°, 25\lambda)$ | $(16.9998°, 24.9829\lambda)$ |
| Source 15 | $(-10°, 9.5\lambda)$ | $(-9.9989°, 9.4979\lambda)$ |
| Source 16 | $(25.5°, 18\lambda)$ | $(25.5000°, 18.0005\lambda)$ |
| Source 17 | $(12.5°, 29\lambda)$ | $(12.5001°, 28.9992\lambda)$ |

can accurately find multiple RNF sources and estimate that the number of sources is larger than the number of array elements in the position estimation results of multiple RNF sources under varied array antennas. In summary, the proposed method significantly enhances the array degree of freedom and can estimate the source position properly in the presence of gain–phase errors.

*5.6. Performance of Mixed Source DOA Estimation.* The applicability of the proposed method in the mixed source localization issue is evaluated using three criteria: the localization results of several trials, the effect of SNR, and the number of snapshots on the RMSE of the source location estimation results. It is assumed that there are RNF and RFF sources with locations $(-15°, 15\lambda)$ and $(20°, 1800\lambda)$ incident to the receiving array and SNR of 20 dB. Figure 12 depicts the results of 500 mixed source position estimations. Figures 13 and 14 exhibit the RMSE impacts of SNR and number of snapshots on the estimate results for mixed source location parameters. In the SNR and snapshot number experiment, TS-MUSIC, PCA, and CRB are compared to the proposed algorithm.

In Figure 12(a) represents the result of 500 tests for estimating the mixed source angle, and Figure 12(b) represents the result of 500 experiments for estimating the mixed source range. The graphic shows that the proposed method is capable of properly estimating the direction of arrival of mixed source. The proposed method can estimate the range parameters of the RNF source with high accuracy, however, it is unable to estimate the range parameters of the RFF source. To differentiate the RNF source from the RFF source, the range parameter estimate results of the RFF source are substantially greater than the borders between the two sources. As a result, the proposed method works well for estimating mixed source positions.

Two graphs representing the RMSE effect curves of SNR and snapshot number on the estimate results of mixed source

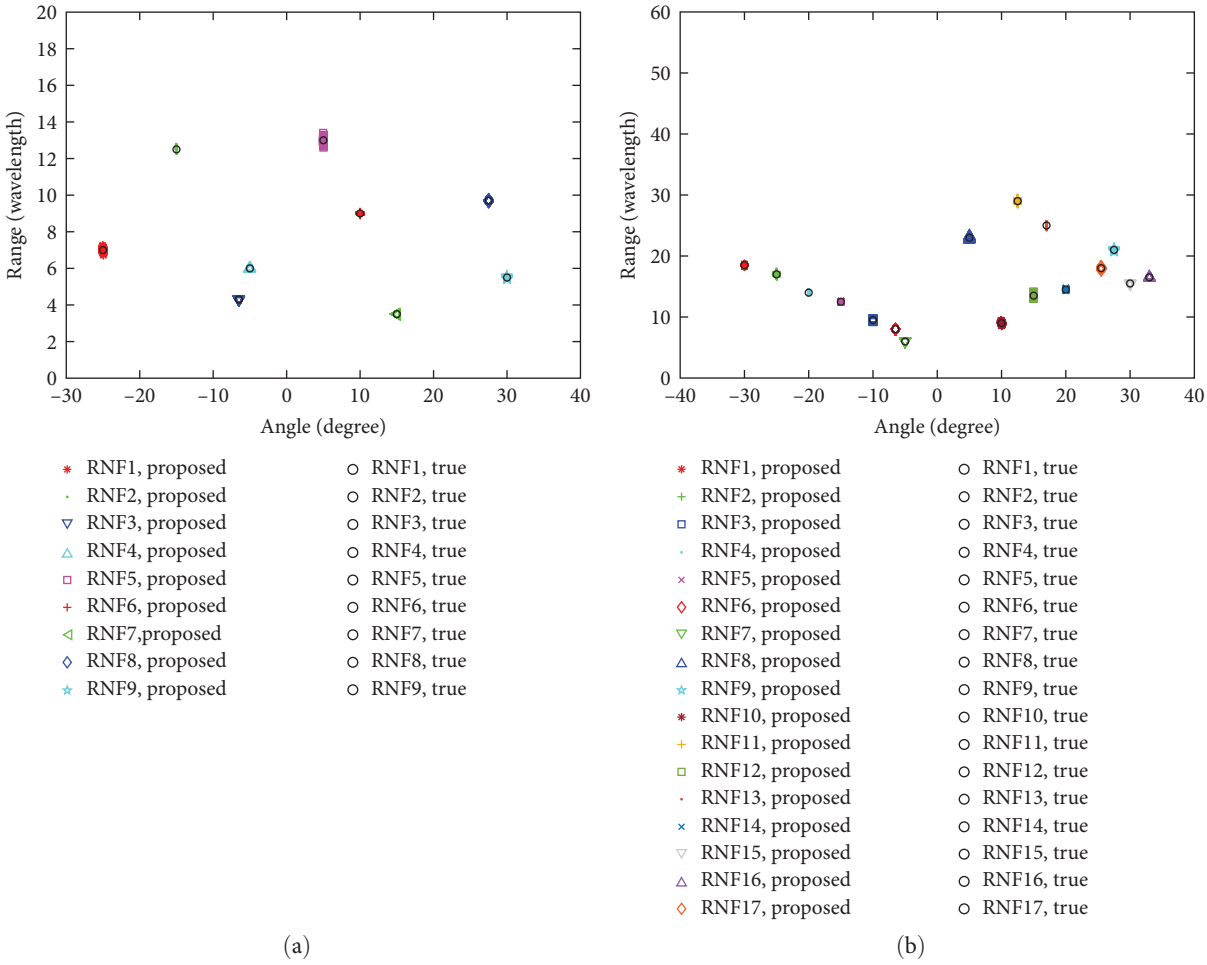


Figure 11: The position estimation results of 500 trials of multiple NF sources. (a) Five array elements. (b) Nine array elements.

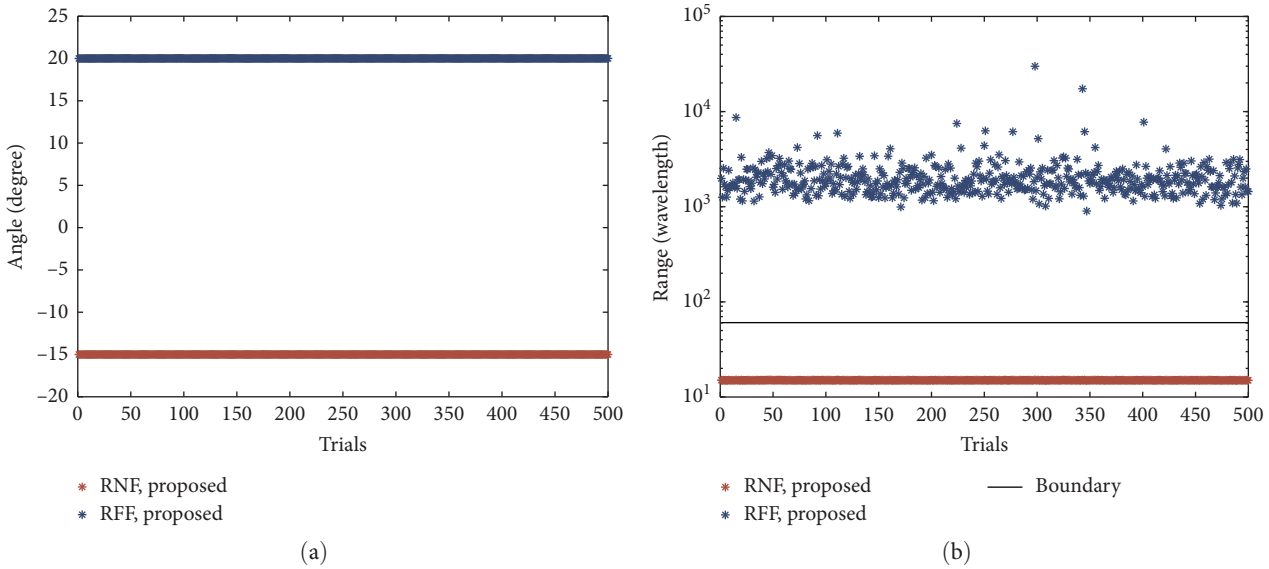


Figure 12: The position estimation results of 500 trials of mixed sources. (a) Angle estimation results. (b) Range estimation results.

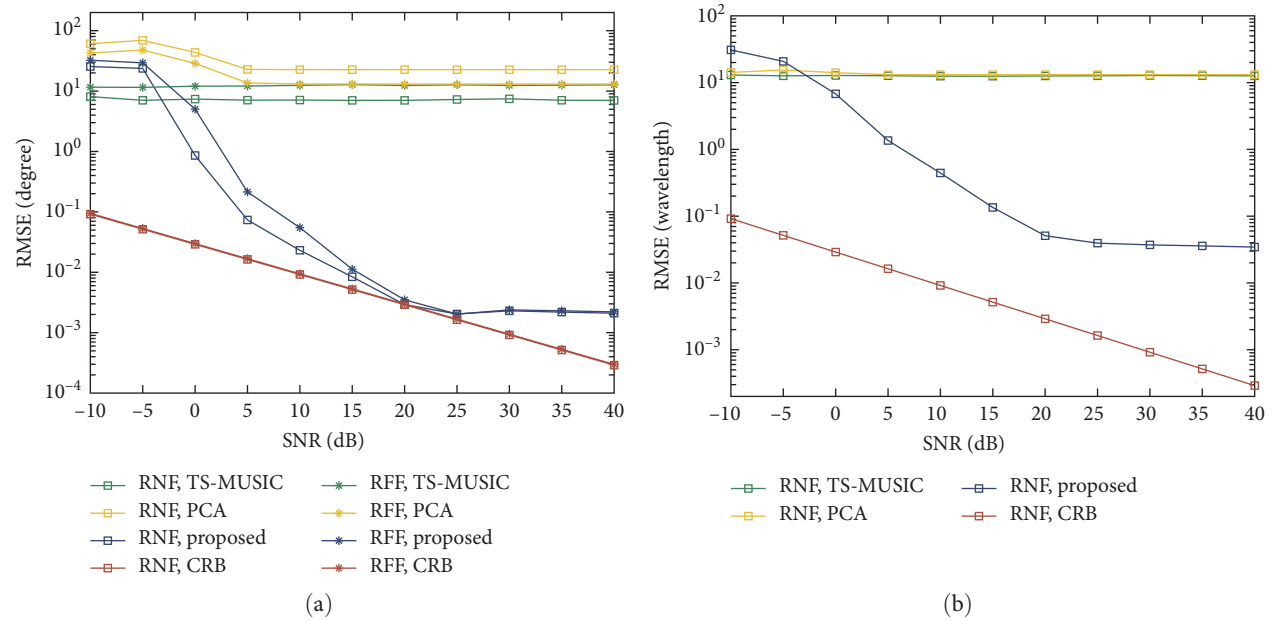


Figure 13: The variation curve of RMSE of mixed source location results with the SNR. (a) RMSE of angle estimation. (b) RMSE of range estimation.

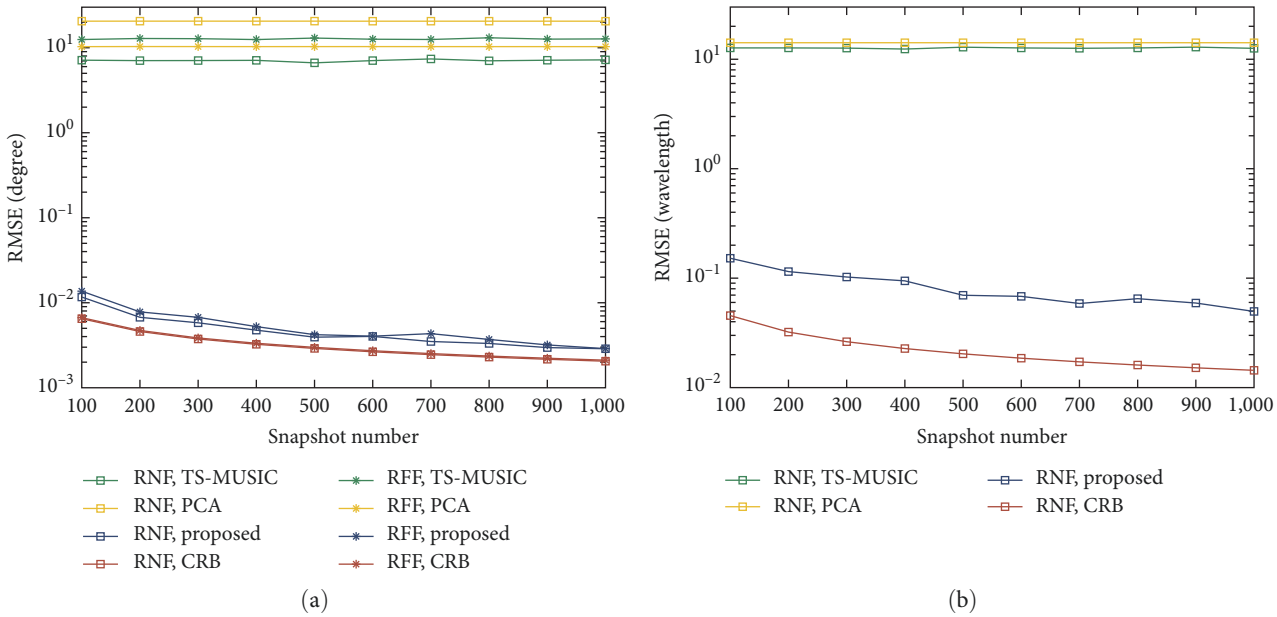


Figure 14: The variation curve of RMSE of source location results with snapshot. (a) RMSE of angle estimation. (b) RMSE of range estimation.

angle parameters and two graphs representing the RMSE influence curves of SNR and snapshot number on the estimation results of RNF source range parameters are shown in Figures 13 and 14. While the proposed method can precisely estimate the direction of arrival of the mixed source and the range parameters of the RNF source, the TS-MUSIC and PCA algorithms are unable to determine the position parameters of the mixed source. In Figures 13(a) and 13(b), the error of the source location estimation results produced by the proposed method diminishes as SNR increases, and the error tends to stabilize when SNR is more than 20 dB. However, it has a lesser error than the source position estimation results produced by the TS-MUSIC and PCA algorithms. In Figures 14(a) and 14(b), the error of the source position estimation results acquired by the proposed method changes slightly with the rise in the number of snapshots. In conclusion, the method proposed in this research can implement the location parameter estimate of the mixed source and is relevant to mixed source scenarios.

## 6. Conclusion

In practical applications, the RNF source localization technique struggles with unpredictable gain phase inaccuracy. The number of array elements determines the maximum number of estimated sources for the majority of the RNF source localization techniques currently in use. This study proposes, for the situation of just reference array elements without gain–phase error, a high degree of freedom RNF source location technique based on accurate model. The degree of freedom of the array is effectively improved by using the time-shift method and creating a new data matrix that complies with the needed structure of TLS-ESPRIT, and the maximum number of estimated sources is no longer constrained by the number of array elements. The RNF and RFF sources are successfully separated by the border between the Fresnel zone and the Fraunhofer zone, and the suggested method is utilized to estimate the position parameters of the mixed source based on the same signal model. The experimental simulation demonstrates that the maximum estimable source number of the proposed algorithm is not constrained by the number of elements and that it is capable of precisely estimating the positions of both RNF and mixed sources. However, when the SNR is less than 5 dB, the source position parameter estimation results have a large error. Therefore, in the future research, we will reduce the source position estimation error under low-SNR conditions on the basis of the algorithm. In addition, the proposed algorithm can only increase the maximum number of estimable sources in the presence of only amplitude and phase errors. However, in the actual environment, there are also array element position errors and mutual coupling errors between array elements. Therefore, how to improve the maximum number of estimated sources of the algorithm when there are multiple errors is also of great significance.

## Data Availability

The data (.C) used to support the findings of this study are available from the corresponding author upon request.

## Conflicts of Interest

The authors have declared that they have no conflicts of interest.

## References

[1] J. Li, Y. Wang, Z. Ren, X. B. Gu, M. Yin, and Z. Wu, "DOA and range estimation using a uniform linear antenna array without a priori knowledge of the source number," *IEEE Transactions on Antennas and Propagation*, vol. 69, no. 5, pp. 2929–2939, 2021.

[2] Z. Zheng, M. Fu, W.-Q. Wang, and H. C. So, "Mixed far-field and near-field source localization based on subarray cross-cumulant," *Signal Processing*, vol. 150, pp. 51–56, 2018.

[3] Q. Bao, W. Hu, and Q. Wang, "A novel multi-site damage localization method based on near-field signal subspace fitting using uniform linear sensor array," *Ultrasonics*, vol. 116, Article ID 106485, 2021.

[4] P. Vallet, X. Mestre, and P. Loubaton, "Performance analysis of an improved MUSIC DoA estimator," *IEEE Transactions on Signal Processing*, vol. 63, no. 23, pp. 6407–6422, 2015.

[5] C. Qian, L. Huang, Y. Xiao, and H. C. So, "Two-step reliability test based unitary root-MUSIC for direction-of-arrival estimation," *Digital Signal Processing*, vol. 44, pp. 68–75, 2015.

[6] J. C. Lin, X. C. Ma, S. F. Yan, and C. P. Hao, "Time–frequency multi-invariance ESPRIT for DOA estimation," *IEEE Antennas and Wireless Propagation Letters*, vol. 15, pp. 770–773, 2016.

[7] M. L. Xiao, Z. B. Duan, and Z. L. Yang, "A weighted forward–backward spatial smoothing DOA estimation algorithm based on TLS-ESPRIT," *IEICE Transactions on Information and Systems*, vol. E104.D, no. 6, pp. 881–884, 2021.

[8] S. Qiu, X. F. Ma, R. L. Zhang, Y. B. Han, and W. X. Sheng, "A dual-resolution unitary ESPRIT method for DOA estimation based on sparse co-prime MIMO radar," *Signal Processing*, vol. 202, Article ID 108753, 2023.

[9] X. L. Su, Z. Liu, T. P. Liu, B. Peng, X. Chen, and X. Li, "Passive localization of mixed near-field and far-field sources without eigendecomposition via uniform circular array," *Circuits, Systems, and Signal Processing*, vol. 39, no. 10, pp. 5298–5317, 2020.

[10] M. D. Kuang, J. Xie, L. Wang, Y. X. Wang, and Y. Y. Gong, "Fast reweighted smoothed $I_0$-norm near-field source localization based on fourth-order statistics," *IEEE Communications Letters*, vol. 26, no. 1, pp. 74–78, 2022.

[11] S. Liu, J. Zhao, Z. Yuan, R. Zhou, M. Xiao, and C. Lu, "Localization for mixed near-field and far-field sources by interlaced nested array," *Progress in Electromagnetics Research M*, vol. 82, pp. 107–115, 2019.

[12] J. Sun, C. Y. Hao, and Z. Zheng, "Passive localization of near-field sources based on overlapped subarrays," *Circuits, Systems, and Signal Processing*, vol. 39, no. 1, pp. 502–512, 2020.

[13] H. Liu, Y. Chen, Y. Lin, and Q. Xiao, "A multiple sources localization method based on tdoa without association ambiguity for near and far mixed field sources," *Circuits, Systems, and Signal Processing*, vol. 40, no. 8, pp. 4018–4046, 2021.

[14] X. H. Wu and J. Yan, "A second-order statistics-based mixed sources localization method with symmetric sparse arrays," *IEEE Communications Letters*, vol. 24, no. 8, pp. 1695–1699, 2020.

[15] J. Liang and D. Liu, "Passive localization of mixed near-field and far-field sources using two-stage music algorithm," *IEEE Transactions on Signal Processing*, vol. 58, no. 1, pp. 108–120, 2010.

[16] Q. Zhang, W. Li, B. Yang, and S. Li, "An auxiliary source-based near field source localization method with sensor position error," *Signal Processing*, vol. 209, Article ID 109039, 2023.

[17] J. Xie, H. Tao, X. Rao, and J. Su, "Localization of mixed far-field and near-field sources under unknown mutual coupling," *Digital Signal Processing*, vol. 50, pp. 229–239, 2016.

[18] K. Wen, Y. Tian, and Z. Dong, "Mixed source localization considering mutual coupling and unknown nonuniform noise under exact spatial geometry," *Signal Processing*, vol. 210, Article ID 109066, 2023.

[19] J. Q. Zhen, "DOA estimation to mixed signals in the presence of gain–phase perturbation," *Mobile Networks and Applications*, vol. 23, no. 4, pp. 743–751, 2018.

[20] H. Ma, H. Tao, and H. Kang, "Mixed far-field and near-field source localization using a linear electromagnetic-vector-

sensor array with gain/phase uncertainties," *IEEE Access*, vol. 9, pp. 132412–132428, 2021.

[21] J. Xu, B. Wang, and F. Hu, "Near-field sources localization in partly calibrated sensor arrays with unknown gains and phases," *IEEE Wireless Communications Letters*, vol. 8, no. 1, pp. 89–92, 2019.

[22] Y. Tian, Y. Wang, X. Rong, and Q. Lian, "Mixed source localization and gain–phase perturbation calibration in partly calibrated symmetric uniform linear arrays," *Signal Processing*, vol. 166, Article ID 107267, 2020.

[23] T. Shu, L. N. Li, and J. He, "Near-field localization for non-circular sources in the presence of sensor phase uncertainties," *IEEE Wireless Communications Letters*, vol. 10, no. 3, pp. 562–566, 2021.

[24] J. He, T. Shu, L. Li, and T.-K. Truong, "Mixed near-field and far-field localization and array calibration with partly calibrated arrays," *IEEE Transactions on Signal Processing*, vol. 70, pp. 2105–2118, 2022.

[25] M. Wax and T. Kailath, "Detection of signals by information theoretic criteria," *IEEE Transactions on Acoustics, Speech, and Signal Processing*, vol. 33, no. 2, pp. 387–392, 1985.

[26] J. Q. Zhen and B. Y. Guo, "DOA estimation for far-field sources in mixed signals with mutual coupling and gain–phase error array," *EURASIP Journal on Wireless Communications and Networking*, vol. 2018, no. 1, 2018.

[27] J. He, L. Li, and T. Shu, "Bearing and range estimation with an exact source-sensor spatial model," *IET Signal Processing*, vol. 14, no. 9, pp. 614–623, 2020.

[28] J. He, L. Li, T. Shu, and T.-K. Truong, "Mixed near-field and far-field source localization based on exact spatial propagation geometry," *IEEE Transactions on Vehicular Technology*, vol. 70, no. 4, pp. 3540–3551, 2021.

[29] R. Roy and T. Kailath, "ESPRIT-estimation of signal parameters via rotational invariance techniques," *IEEE Transactions on Acoustics, Speech, and Signal Processing*, vol. 37, no. 7, pp. 984–995, 1989.

[30] R. Schmidt, "Multiple emitter location and signal parameter estimation," *IEEE Transactions on Antennas and Propagation*, vol. 34, no. 3, pp. 276–280, 1986.